Journal of Fluids and Structures (1998) **12,** 131–151

REVERSAL OF THE BERNOULLI EFFECT AND CHANNEL FLUTTER

L. HUANG

Department of Mechanical Engineering, The Hong Kong Polytechnic University Kowloon, Hong Kong

(Received 13 February 1997 and in revised form 23 October 1997)

This paper is concerned with the collapse and subsequent self-excited oscillation of compliant tubes conveying fluids. Our model considers a two-dimensional, inviscid, shear flow in a flexible channel of infinite length subject to linear, travelling varicose waves. Analysis of the boundary-value problem leads to two findings which do not seem to have been noticed before, despite the close attention this kind of fluid–structure interaction has attracted on account of its medical significance. The pressure perturbation on the wall has two components, the first is in-phase with the wall displacement and the second with the velocity of the wall motion. For potential flow, the first component is the only one tending to destabilize and is known as the Bernoulli effect. For shear flow, however, the sign of the pressure is reversed as the Bernoulli effect is overcome by the perturbations of the vorticity field. Streamline patterns show that Kelvin's "cats' eyes" are sheltered in the wider channel sections, rendering the effective flow passage smaller where the physical width is larger. The second component produces a wave drag, hence irreversible transfer of energy from the flow to waves. We argue that this is a possible mechanism for the self-excited oscillation observed in experiments. This mechanism is similar to Miles's (1957) mechanism of water wave generation by wind, which is a class B instability according to the Benjamin–Landahl categorization, but the accompanying reversal of the Bernoulli effect is different and depends essentially on the presence of a second boundary. The eigenvalue problem is also considered and it is shown that dynamic instability of long but finite wavelength could be experienced by compliant channels with thick walls, a typical application being the respiratory flow in the upper airways. The critical flow speed is given in terms of the channel properties.

1. A BRIEF REVIEW

THE PROBLEMS OF STABILITY of flexible structures exposed to fluid flows have tremendous geometrical variety and involve several distinct fluid–structure interaction mechanisms. Two typical problems are (i) flow over a single flexible surface such as the air–sea interface, and (ii) flow through collapsible tubes such as the flow of the blood and air in human bodies. Though closely related, theoretical developments in the two areas have distinct features. Much can be learned from a comparative study of the two topics. In what follows, we first give a brief view of experiments and theories pertaining to the internal flow, followed by a similar account for the external flow. We then ask the question of whether the well-established theory of travelling wave flutter in the external flow has its equivalent in the internal flow. This leads us to a new model of shear flow through a compliant channel, a model with interesting and different properties.

0889-9746/98/020131 + 21 $25.00/fl970131

1.1. Flow Through Collapsible Tubes

Studies of flow through collapsible tubes are motivated by many physiological phenomena relating to blood flow and respiration, as well as industrial concerns with oil pipelines. Virtually, all fluid-carrying vessels in the body are elastic and collapsible. Two such examples are the pulmonary blood vessels in the upper levels of the lung (Caro *et al.* 1978) and the bronchial airways (Grotberg 1994). Recently, human snoring has been added to the category (Huang *et al.* 1995). About 15% of the adult population snore and when they do, or rather we do, the upper airways routinely collapse and oscillate under excessive breathing effort. One remarkable characteristic of snoring is that it occurs while the inspiratory flow rate is still increasing whereas other phenomena, such as wheezing (Gavriely *et al.* 1989), start after the volume flow rate becomes limited. Many people also suffer from a medical condition called "obstructive sleep apnoea", where "sleep apnoea" is defined as a total cessation of breathing for more than 10 s, causing life-threatening oxygen desaturation. The pathogenesis of apnoea is still a mystery, but it seems reasonable to suggest that the airway collapse is a prelude.

Mechanical modelling for different physiological phenomena must deal with different ranges of the important fluid–structure coupling parameters, such as the mass ratio and the strength of the wall compared with the dynamic head of the flow, but laboratory models are remarkably similar in their basic construction. A typical rig has a segment of rubber tube clamped at its up and downstream ends and surrounded by a pressure chamber which controls the transmural pressure. Devices may be added to provide independent adjustments on the driving pressure and the flow resistance (such a design is traditionally called a 'Starling resistor"). Due to friction, the flow at the downstream end of the tube has the lowest pressure and at a certain volume flow rate the tube first buckles near the downstream clamp forming a "neck". Further decrease in the downstream pressure accelerates the flow but narrows the neck, and a point will be reached when the volume flow rate attains its peak value. Upon further increase in the driving pressure, oscillations of several distinct frequencies as well as random vibrations may follow [see a review by Kamm & Pedley (1989), and extensive experiments by Bertram *et al.* (1990)]. It is not clear whether the oscillation is a nonlinear manifestation of static instability or an intrinsically linear dynamic instability.

It may seem too idealistic for modelling any real physiological phenomena, but the Starling resistor is by no means free of theoretical complications. The transmural pressure is nonuniform along the tube length. The flow around the neck probably involves unsteady separation and is poorly understood. Theories based on empirical models for the flow separation have been developed (Cancelli & Pedley 1985), but their direct validation by experiments is still difficult (Jensen 1990). Vortex shedding may be a factor for which progress has been made by numerical simulations (Luo & Pedley 1996) of flow through a channel with a segment of massless wall under tension. But for a more realistic wall and perhaps in three dimensions, the stress distribution in a collapsed shell presents a daunting task for solid mechanics (Heil & Pedley 1995). One is often forced to use a one-dimensional fluid–structure coupling model, the tube law, which assumes a stiffness coefficient relating the local transmural pressure with the cross-sectional area, e.g. Shapiro (1977) and Cancelli & Pedley (1985). To find a credible lumped-stiffness coefficient, one has to integrate the structural restoring forces along the circumference. As the tube collapses, the circumferential bending stiffness, being proportional to local curvature, decreases dramatically as the initially circular section changes into elliptical shapes with large aspect ratio which may be modelled by a two-dimensional channel [cf. Kececioglu *et al.* (1981; Figures 7 & 8)]. In fact,

a Starling resistor is a system of highly variable parameters. True to physiological reality it may be, but these theoretical complications often represent an obstacle to a clear analytical understanding of the oscillations.

A more idealized and more tractable theoretical model is constructed by Grotberg & Reiss (1984) [for later publications on this theory, see Grotberg & Shee (1985), Grotberg & Gavriely (1989), Gavriely *et al.* (1989) and Grotberg (1994)]. It assumes a uniform transmural pressure and a plug flow as the core. The key new element is the inclusion of the viscous effect by a Darcy friction coefficient which leads to travelling wave flutter, whereas a potential flow model only gives static divergence. Recently, LaRose & Grotberg (1997) have abandoned this crude model and taken the theory forward to the realistic velocity profile in developing flows. More details are given in Section 1.3, and a direct comparison with our theory will be presented in Section 3.2.

Interest in oil pipelines and other engineering applications have also led to extensive research in internal flow as well as annular flow through coaxial cylindrical shells (Païdoussis & Issid 1974; Weaver & Païdoussis 1977). Among many recent papers in this area is the numerical simulation using the linearized, unsteady flow Navier–Stokes equation (Nguyen *et al.* 1994).

In yet another separate development, Kumaran *et al.* (1994) and Kumaran (1995*a*) studied the destabilizing mechanism in Stokes flow through flexible tubes lined with a gel-like viscoelastic medium. The coupling between the fluid shear stress and the tangential motion of the fluid–solid interface is shown to be responsible for the interface instabilities. In these studies, the inertia of both fluid and solid is ignored and there is no coupling between the mean flow and the fluctuations in directions normal to the fluid–solid interface. The effect of fluid inertia was analysed later (Kumaran 1995b, 1996), with the interesting finding that the above-mentioned destabilizing mechanism is neutralized by the stabilizing effect of viscous damping in high Reynolds number flows. Although the tangential motion of the wall is neglected in our studies for walls with high shear elastic modulus, Kumaran's findings on the differences between the instabilities of flow through flexible tubes and the much more widely investigated configuration of channels may prove to be very useful in the future development of theory into three dimensions.

1.2. External Flow Instabilities

Linear instability of flow over a rigid surface, the Tollmien–Schlichting instability (TSI), concerns the early stages of flow transition from laminar to turbulent and the governing equation is the Orr–Sommerfeld equation. The key to TSI is the production of positive Reynolds stress, hence energy transfer from the mean flow to the perturbation, by the wall friction layer enforcing the no-slip condition on the tangential wave perturbations. Kramer's (1957) claim of substantial drag reduction by dolphin-skin-like flexible surfaces provided the motivation for extensive theoretical studies on the effect of flexible boundaries on flow instability. Brooke Benjamin (1960) showed that the response from a flexible surface can disrupt the mechanism of TSI by effectively removing the friction layer, thus creating a delay in boundary-layer transition.

The second type of instability that may occur in a flexible surface is the travelling wave flutter (TWF). Its essential fluid dynamic mechanism was first discovered by Miles (1957) in the context of water wave generation by wind. The irreversible energy transfer from the mean airflow to the wavy motion of water is found within the gradient of vorticity at the critical layer where the mean flow speed is equal to the wave speed. This mechanism

operates even if the fluid is inviscid. It was later re-examined in the framework of viscous flow by Brooke Benjamin (1959) and by Miles (1959) himself, both confirming that there is little influence of viscosity. Brooke Benjamin (1963) later classified this essentially inviscid mechanism as a class B instability (flexibility-modified-TSI being class A), which has to be carefully avoided if a Kramer-type surface is to succeed in delaying the onset of class A instability.

In fact, Brooke Benjamin went on to name the static divergence and Kelvin– Helmholtz instability as class C instabilities [see also Landahl (1962) for an illuminating categorization in terms of system energy balance]. One of the main contributions from Brooke Benjamin, however, is his discovery of the destabilizing effect that structural damping has on class A waves, which is in sharp contrast to the stabilizing role it normally plays in instabilities such as TWF. Furthermore, fluid viscosity could bring about a resonance or coalescence of class A and B instabilities, but this was found to be unlikely by Miles (1962) in normal circumstances of water wave generation. The theory was further developed and clarified by Carpenter & Garrad (1985, 1986), who classified it as a fourth type of instability. But for the purpose of our comparative studies, it may be sufficient to sum up by stating that the fundamental sources of the class A, B and C instabilities are, respectively, fluid viscosity, vorticity gradient and fluid inertia. These three distinct physical mechanisms will now guide us to re-examine some existing instability theories pertaining to internal flow and lead us to a new model.

1.3. Introduction of the Internal Shear Flow Model

Until quite recently the "diffusion" of theories of external flow instability into studies of internal flow seems to have been limited to the class A instability. Applying the Orr–Sommerfeld analysis to the channel flow with flexible walls, Hains & Price (1962), and later Green & Ellen (1972), found that, as in external flows, TSI is also delayed in flexible channels and can be eliminated by sufficient wall flexibility. In practice, however, there are perturbations, like surface roughness and finite amplitude perturbations, that readily promote flow transition at a Reynolds number much lower than that predicted by a linear Orr–Sommerfeld theory [see, for example, Rotenberry & Saffman (1990) and Rotenberry (1992)]. A recent numerical simulation based on the Orr–Sommerfeld equation (Davies & Carpenter 1997) also suggests that laminar-turbulent transition could be delayed indefinitely with multiple short compliant panels.

Two points need to be clarified regarding TSI in channel flows. First, TSI is only found for the antisymmetric perturbation mode in which the axial perturbation velocities on the two walls are in opposite directions, which differs from the symmetric mode considered by our shear flow theory. None of the aforementioned work covers the symmetric mode. The second point is that, when a flexibility-modified-TSI occurs, say, at a higher Reynolds number, it leads to flow transition but not necessarily to violent flutter involving substantial vertical motion on the part of the flexible surfaces. The fact that this is so can be explained more clearly by nonlinear theories (Bayly *et al.* 1988). First, the positive growth rate available from the TSI mechanism is very limited and waves settle down to a mild finite amplitude, which is itself a dynamic mean state where the growth of further perturbation constitutes a secondary instability. The final stages of turbulence transition feature the growth of short waves, which bear little resemblance to the long waves predicted by the linear TSI and which are unlikely to couple with the wall vibration. It is perhaps not difficult to appreciate this point from the fact that Tollmien–Schlichting waves primarily exist in flows over rigid boundaries.

Static divergence can also be anticipated in a channel flow with sufficiently high flow speed and a structural damping so high that flutter is not encountered first. This type of instability was the only result available to earlier biofluid-mechanical studies based on potential flow models [e.g., Conrad (1969); Matsuzaki & Fung (1979)]. Again, the perturbation considered for divergence is in a symmetric mode.

Knowing that the linear instabilities of classes A and C exist in flexible channel flows, we naturally ask the question of whether the essentially inviscid mechanism of travelling wave flutter (class B) also exists in channel flows. To answer this, we exclude class A instability and its possible interaction with class B, but class C instability, being insensitive to damping, can be considered alongside. Therefore we introduce a model in which (a) the fluid can be treated as inviscid since viscosity is not essential for class B or C instabilities; (b) the flexible channel is uniform and of infinite length; its two walls are perturbed to move in the opposite directions (symmetric mode), and it is hoped that results from such a two-dimensional configuration will be relevant to the flutter of partially collapsed tubes where the aspect ratio may be very high. It is anticipated that structural viscosity stabilizes class B instability, so the main point we want to know is whether the mechanism of energy transfer from the fluid to the surface is present. The possibility of a class C instability will also be evident once we know whether the pressure response to the channel wall perturbation increases or decreases the effective bending stiffness of the wall.

In what follows, we adapt Miles's (1957) theory to our model of shear flow through flexible channels. We find that the mechanism of class B instability in symmetric mode indeed exists, and our preliminary eigenvalue studies show that travelling wave flutter occurs when the rate of energy transfer from the flow to the wall vibration exceeds the rate of structural dissipation. Furthermore, for velocity profiles with moderate gradient near the wall, such as the plane Poiseuille flow, the pressure induced by a travelling varicose wave opposes the wall displacement as part of the perturbation Reynolds stress overrides the inertia force. In other words, the familiar Bernoulli effect is reversed.

Recently, LaRose & Groberg (1997) considered very much the same model except that the fluid viscosity is retained. They solve the eigenvalue problem based on the Orr–Sommerfeld equation both numerically and, for the long-wave limit, analytically. They confirmed the existence of the travelling-wave flutter in flexible channels and many results agree with our analytical solution for the inviscid flow model. However, there are differences, the main one being the flutter wave speed. In our model, the wave speed should be less than the maximum flow speed at the channel centreline, while theirs indicates that the critical wave speed is typically twice as much as the maximum flow speed.

2. VARICOSE WAVE THEORY

2.1. The Boundary-Value Problem

We consider a two-dimensional, inviscid, incompressible shear flow through an elastic channel of infinite length. The two channel walls undergo varicose heaving motions of small, constant amplitude in the form of a travelling wave. The wave travels in the direction of the flow and its phase speed is less than the maximum undisturbed flow speed. The reason for limiting the wave speed in this range will be given shortly. We now want to find out the pressure perturbation on the walls.

As shown in Figure 1, the channel has a height of $2h^*$. The undisturbed flow has its maximum speed at the centre, $U^*_{\max}$, and for the lower part, $y^* \in (0, h^*)$, the undisturbed vorticity $\mathrm{d}U^*/\mathrm{d}y^*$ decreases with height to vanish at $y^* = h^*$.

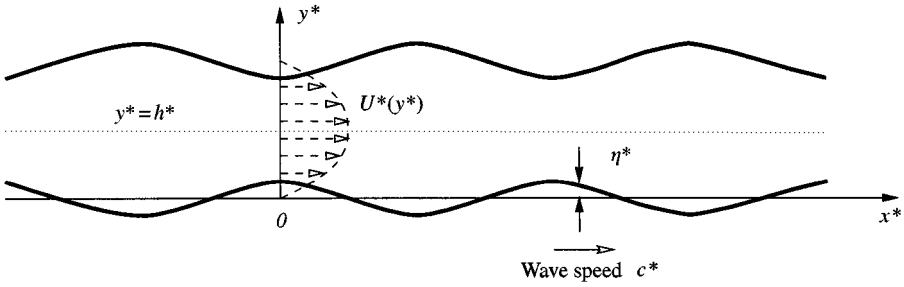

Figure 1. The model problem

We now scale all dimensional variables in terms of length h^*, velocity $U^*_{\max}$ and pressure head $\rho_0^*(U^*_{\max})^2$, where ρ_0^* is the constant fluid density. The dimensionless variables are denoted by corresponding dimensional symbols without the asterisk. Note that h and $U|_{y=1}$ are unity by definition.

The elevation of the lower wall is prescribed as the real part of

$$\eta = \eta_0 e^{ik(x-ct)}, \tag{1}$$

where the wave number k and the wave speed c are both real and the scaled wave amplitude $\eta_0 \ll 1$. The coupled fluid–wall eigensystem will be investigated later when c will have to be assumed to be complex. The linear perturbation is governed by the Rayleigh equation, which is briefly derived below, since the original momentum conservation equations will prove to be handy when interpreting the physics.

The Euler momentum equation is

$$\frac{D\boldsymbol{q}}{Dt} + \nabla p = 0,$$

where $\boldsymbol{q} = (U + u, v)$ is the complete velocity and p is the perturbation pressure. Linearization gives

$$\frac{\partial u}{\partial t} + U\frac{\partial u}{\partial x} + v\frac{dU}{dy} + \frac{\partial p}{\partial x} = 0, \quad \frac{\partial v}{\partial t} + U\frac{\partial v}{\partial x} + \frac{\partial p}{\partial y} = 0. \tag{2}$$

The conservation of mass is automatically satisfied by the introduction of a perturbation stream function ψ as follows:

$$\psi(x, y, t) = \Psi(y)\eta(x, t), \quad u = \frac{\partial \psi}{\partial y}, \quad v = -\frac{\partial \psi}{\partial x}, \tag{3}$$

where, for convenience, a factor of η has been taken out of ψ; so, the function $\Psi(y)$, which represents the vertical structure of ψ, has the dimension of velocity and is on the order of unity. The integration of the axial momentum equation in (2) gives the pressure perturbation

$$p = -[(U - c)\Psi' - U'\Psi]\eta, \tag{4}$$

which, when inserted for $\partial p/\partial y$ in the vertical momentum equation, yields the Rayleigh equation:

$$[(U - c)\Psi' - U'\Psi]' = k^2(U - c)\Psi, \tag{5}$$

where primes denote differentiation with respect to y.

The first boundary condition is the continuity of vertical velocity on the lower wall:

$$\frac{\partial \eta}{\partial t} + U\frac{\partial \eta}{\partial x} = \mathrm{i}k[U(0) - c]\eta = v = -\frac{\partial(\Psi\eta)}{\partial x} = -\mathrm{i}k\Psi\eta,$$

so that $\Psi(0) = c - U(0)$. We may assume a no-slip condition on the wall for the mean shear flow, $U(0) = 0$, so that $\Psi(0) = c$, bearing in mind that the same is not imposed on the perturbation velocity u in an inviscid flow model.

The second boundary condition concerns the symmetric motion of the two opposing walls which allows no flow across the centreline, so that $v = -\partial(\Psi\eta)/\partial x = -\mathrm{i}k(\Psi\eta) = 0$ at $y = 1$. The two boundary conditions are now written as

$$\Psi(0) = c, \quad \Psi(1) = 0. \tag{6}$$

The pressure on the wall is of primary interest, but first we have a look at the pressure expression for all levels given in equation (4). There are two terms inside the square bracket, the first is the inertia term (Bernoulli effect), and the second the effect of the mean flow vorticity. The physics of the latter may be appreciated by changing to a reference frame which rotates with an angular velocity of $\frac{1}{2}U'$ [cf. Lighthill (1962, p. 389)]. The flow then appears to be locally irrotational. Such a change renders the Bernoulli equation applicable only at the expense of introducing the Coriolis force to the vertical perturbation, which is exactly the second part of the perturbation pressure given in equation (4). The Rayleigh equation is basically a statement of the force balance between the pressure gradient and the inertia force in the vertical direction. The vertical pressure gradient vanishes in the long-wave limit, $k \to 0$, as can be seen from equations (4) and (5), and the pressure on the wall is the same as at any other level. For either $y = 0$ or $y = 1$, we may make use of one of boundary conditions (6), so that

$$p|_{y=0} = c[\Psi'(0) + U'(0)]\eta, \quad p|_{y=1} = -(1 - c)u|_{y=1}.$$

The last equation means that the Bernoulli equation applies on the centreline because the axial component of the vorticity-related force, $-U'v$, vanishes. Note that equating the pressure at $y = 1$ to that at $y = 0$ by virtue of the long-wave limit is not equivalent to conducting a one-dimensional flow analysis. The difference, which is an important one, lies in that $u|_{y=1}$ has a certain phase delay in relation to $u|_{y=0}$ in two-dimensional shear flows.

The main difficulty in solving the governing equation (5) is that a singularity occurs at the critical layer, $y = y_c$, where the wave speed equals the shear flow speed, $U(y_c) = c$. The singularity is removed by the inclusion of viscosity, which then gives the fourth-order Orr–Sommerfeld equation. Normally there is no explicit solution of compact form even for the Rayleigh equation for arbitrary velocity profiles. The method of Frobenius is often used for a series solution around a regular singularity. An alternative procedure is Heisenberg's expansion (Lin 1955, p. 34) in terms of k^2, where k is the wave number, so that the stream function and the wall pressure are, respectively,

$$\Psi = \Psi_0 + \Psi_2 k^2 + \Psi_4 k^4 + \cdots, \quad p|_{y=0} = p_0 + p_2 k^2 + p_4 k^4 + \cdots. \tag{7}$$

We shall focus on the leading-order terms Ψ_0 and p_0, whose subscripts should not be confused with the wall location $y = 0$, but the k^2-term will also be given to facilitate the eigenvalue studies later on. The results of the eigenvalue studies will show that perturbations of long but finite wavelength do feature in flutter-type instability in channels with

thick walls. This covers the typical situation of respiratory flow through the upper airways, which is one of our main interests.

At the long-wave limit, the Rayleigh equation (5) is reduced to a first-order ordinary differential equation, $(U-c)\Psi' - U'\Psi = \text{constant}$, where the constant is essentially the pressure perturbation. The solution that satisfies the two boundary conditions (6) is

$$\Psi_0 = -(U-c)\frac{I(1)-I(y)}{I(1)-I(0)}, \quad I(y) = \int \frac{\mathrm{d}y}{(U-c)^2}. \tag{8}$$

A similar expression was used by Brooke Benjamin (1959; eq. 7.4), who remarked that the extra terms present in the full Heisenberg expansion do not affect the behaviour of the shear flow in any vital way. Before we specify the velocity profile $U(y)$, we would like to carry out some general investigations on the solution.

2.2. General Investigations on the Long-Wave Solution

The singular integrand $(U-c)^{-2}$ can be expressed by its Lorentz series around $y = y_c$,

$$\frac{1}{(U-c)^2} = \frac{1}{(U_c')^2}\left\{\frac{1}{(y-y_c)^2} - \frac{U_c''}{U_c'}\frac{1}{y-y_c} + \left[\frac{3}{4}\left(\frac{U_c''}{U_c'}\right)^2 - \frac{U_c'''}{3U_c'}\right] + \mathcal{O}(y-y_c)\right\},$$

where all subscripts c indicate evaluation on the critical layer $y = y_c$. The integral of the first-order singular term, $(y-y_c)^{-1}$, gives $\ln(y-y_c)$ which has a branch point at $y = y_c$, and the choice of branch is decisive for the outcome. The right choice is made in accordance with the fact that the fluid is viscous, therefore the inviscid solution should be the limit solution for the Orr–Sommerfeld equation. It has been shown that the correct branch is found if the real wave speed c is taken as the limit of a complex one $c = c_r + \mathrm{i}c_i$ as $c_i \to 0$ from the side of wave growth, $c_i > 0$. This means that $y - y_c$, which originates from $(U-c) \approx U_c'(y-y_c)$ near $y = y_c$, has a vanishing negative imaginary part, equivalent to taking a semi-circle route under the singularity when integrating $\int (U-c)^{-2}\,\mathrm{d}y$ along the real axis y by the theorem of residues. It works out to be, for $y < y_c$,

$$\ln(y-y_c) = \ln|y-y_c| - \mathrm{i}\pi \tag{9}$$

(Lin 1955; eq. 8.3.1). The physical significance of the choice is that the inviscid solution is a valid approximation to the viscous problem only when the neutrally stable waves are approached as exponentially growing waves of vanishing growth rate. We will find in our solution that the perturbation waves always tend to grow, although the same is not true for shear flows through rigid channels.

We now proceed to evaluate the integral $I(y)$,

$$I(y) = \frac{1}{(U_c')^2}\left\{\frac{-1}{y-y_c} - \frac{U_c''}{U_c'}\ln(y-y_c) + \left[\frac{3}{4}\left(\frac{U_c''}{U_c'}\right)^2 - \frac{U_c'''}{3U_c'}\right](y-y_c) + \mathcal{O}[(y-y_c)^2]\right\}. \tag{10}$$

The insertion of this result into equation (8) gives $\Psi_0(y)$. Of particular interest is Ψ_0 around the singular point $y = y_c$. By approximating $U-c$ in the first equation of equations (8) by $U_c'(y-y_c)$ and noting that both $I(0)$ and $I(1)$ are finite, we have

$$\Psi_0 = \frac{U_c' + U_c''(y-y_c)\ln(y-y_c) + \mathcal{O}(y-y_c)}{-(U_c')^2[I(1)-I(0)]},$$

and its value at $y = y_c$,

$$\Psi_{0c} = \frac{1}{-U_c'[I(1) - I(0)]}, \tag{11}$$

is finite. For locations near $y = y_c$ we have

$$\Psi_0 = \Psi_{0c}\left[1 + \frac{U_c''}{U_c'}(y - y_c)\ln(y - y_c) + \mathcal{O}(y - y_c)\right], \tag{12}$$

which is the same as that worked out by Rayleigh himself (Miles 1957; p. 193). The derivative Ψ_0' has a logarithmic singularity,

$$\Psi_0' = \frac{\Psi_{0c}U_c''}{U_c'}[\ln(y - y_c) + \mathcal{O}(1)],$$

which indicates a large axial velocity perturbation on the critical layer where sheet-vortices are formed in the absence of viscosity. But the difference between the derivatives on the two sides is found to be finite. Applying the branch point choice equation (9), we have the 'slip velocity',

$$u(y_c^+) - u(y_c^-) = [\Psi_0'(y_c^+) - \Psi_0'(y_c^-)]\eta = \mathrm{i}\pi\frac{\Psi_{0c}U_c''}{U_c'}\eta, \tag{13}$$

which is out-of-phase with the stream function $\psi_{0c}(x) = \Psi_{0c}\eta$.

Having arrived at the asymptotic solution around the critical layer, we are able to evaluate the pressure on the critical layer, p_{0c}. There are two terms in the general expression of pressure, equation (4). The first term $(U - c)\Psi_0'$ vanishes since $U - c \approx U_c'(y - y_c)$ approaches zero faster than the logarithmic divergence of Ψ_0'. Only the vorticity term $U'\Psi_0$ is left. Together with Ψ_{0c} of equation (11), we have

$$p_{0c} = U_c'\psi_{0c}(x) = \frac{-\eta}{\int_0^1 (U - c)^{-2}\,\mathrm{d}y}. \tag{14}$$

Note that the expression is accurate for the critical layer, although it is a long-wave approximation of pressure for other levels, and that the pressure troughs coincide with those of $\psi_{0c}(x)$.

Again, applying the branch point choice, equation (9), for the evaluation of $I(0)$ in equation (11), the long-wave pressure given by equation (14) becomes

$$p_0 = \frac{(U_c')^2\eta}{P_r + iP_i} = \frac{(U_c')^2}{P_r^2 + P_i^2}\left[P_r\eta - \frac{P_i}{k}\frac{\partial\eta}{\partial x}\right], \tag{15}$$

where

$$P_r = \frac{1}{y_c(1 - y_c)} + \frac{U_c''}{U_c'}\ln\left(\frac{1 - y_c}{y_c}\right) + \left[\frac{U_c'''}{3U_c'} - \frac{3}{4}\left(\frac{U_c''}{U_c'}\right)^2\right] + \mathcal{O}[(y - y_c)^2] \tag{16}$$

and

$$P_i = 2\pi\frac{U_c''}{U_c'}, \tag{17}$$

both being real quantities. The pressure has two components, as shown on the right-hand side of equation (15); the first is in-phase with the displacement η, which gives the wall a virtual stiffness providing a linear restoring force, and the second is out-of-phase with η but in-phase with the wave slope $\partial\eta/\partial x$, which gives rise to the wave drag defined as $\int p(\partial\eta/\partial x)\,\mathrm{d}x$. For a travelling wave, the velocity of the wall motion is linked with the slope by $\partial\eta/\partial t = -c\,(\partial\eta/\partial x)$, so that the power transfer from the flow to the wall, $\int(-p)\,(\partial\eta/\partial t)\,\mathrm{d}x$, is simply the wave drag times the wave speed c. Since $U_c'' < 0$ and $P_i < 0$, the wave drag, being proportional to the imaginary part of p_0 in equation (15), is always positive, so is the rate of energy transfer from the flow to the wall vibration. This energy transfer can be regarded as negative virtual damping, which, whenever exceeding the positive structural damping, brings about flutter-type instability for $k > 0$.

If the varicose wave travels faster than the maximum flow speed, $c > 1$, or against the flow, $c < 0$, there is no critical layer and the integrand $(U-c)^{-2}$ in equation (8) has no singularity. As a result, $\Psi(y)$ will be purely real and the wall pressure will act in-phase with the displacement η. It can be seen later in the eigenvalue studies that such waves do not lead to flutter. The same applies to irrotational and uniform flow with any wave speed; the perturbation pressure is then

$$p|_{\text{potential flow}} = -(U-c)^2\eta. \tag{18}$$

The pressure induced by the wall displacement in potential flows always leads, and when this force overcomes the natural stiffness of the structure, the structure fails by static divergence. We are intrigued to find out whether this is also true for elastic channels conveying shear flows. In our formulation, we are looking for a condition under which P_r becomes positive. It is apparent from equation (16) that a simple necessary condition is difficult to obtain, since P_r depends on both the velocity profile and the wave speed. We are content with some qualitative analysis for certain values of the wave speed by specifying y_c. The simplest case is $y_c = \frac{1}{2}$, for which the logarithmic term in equation (16) vanishes and the third term largely determines P_r. Furthermore, we assume a general power law for the mean velocity profile [as was done by Brooke Benjamin (1959), the possibility of turbulence-wave interaction is ignored here],

$$U = y^{1/n}. \tag{19}$$

The dependence of P_r on n is found to be

$$P_r \approx \frac{-n^2 + 6n - 1}{3n^2}.$$

P_r becomes positive when $n < 3 + \sqrt{8} \approx 5.83$, which is indicative of a velocity profile somewhere between laminar and fully turbulent flows. We therefore conclude that for laminar-type flows, P_r can be positive and as a result the fluid exerts a positive virtual stiffness on the displaced channel walls. In other words, the negative stiffness caused by the Bernoulli effect can be reversed depending on the velocity profile and the wave speed.

2.3. The k^2-Term

From the Rayleigh equation (5), we have the following relation for $\Psi_2(y)$ in the Heisenberg expansion of the stream function, $\Psi_0 + k^2\Psi_2 + \cdots$:

$$[(U-c)\Psi_2' - U'\Psi_2]' = (U-c)\Psi_0, \tag{20}$$

where the long-wave stream function Ψ_0 is already given in equation (8). Integrating the above equation twice leads to

$$\Psi_2' - \frac{U'}{U-c}\Psi_2 = \frac{1}{U-c}\left[b_0 + \int_0^y [U(y_1)-c]\,\Psi_0(y_1)\,\mathrm{d}y_1\right], \tag{21}$$

$$\Psi_2 = (U-c)\left\{b_1 + b_0[I(y)-I(0)] + \int_0^y \frac{1}{[U(y_2)-c]^2} \times\left[\int_0^{y_2}[U(y_1)-c]\,\Psi_0(y_1)\,\mathrm{d}y_1\right]\mathrm{d}y_2\right\},$$

where $I(y)$ was defined earlier in equation (8), and b_0 and b_1 are constants to be determined by boundary conditions. By exchanging the order of integration we arrive at

$$\Psi_2(y) = (U-c)\left[b_1 + b_0[I(y)-I(0)] + \int_0^y [U(y_1)-c]\,\Psi_0(y_1)[I(y)-I(y_1)]\,\mathrm{d}y_1\right]. \tag{22}$$

The boundary conditions for Ψ_2 at $y = 0, 1$ are homogeneous since the kinematic condition $v = \mathrm{d}\eta/\mathrm{d}t$ has already been satisfied by the long-wave solution, $\Psi_0(0) = c$. The wall boundary condition $\Psi_2(0) = 0$ gives $b_1 = 0$, while that of the centreline, $y = 1$, gives

$$b_0 = \frac{\int_0^1 [U(y_1)-c]\Psi(y_1)[I(1)-I(y_1)]\,\mathrm{d}y_1}{I(0)-I(1)} = \int_0^1 \Psi_0^2(y_1)\,\mathrm{d}y_1 \tag{23}$$

by recalling the definition of Ψ_0 in equation (8).

The stream function $\Psi_2(y)$ can now be evaluated by equation (22). The contribution of Ψ_2 to the wall pressure, p_2, is found by substituting the expression of Ψ_2 and the boundary condition $\Psi_2(0) = 0$ into the general form of pressure perturbation given in equation (4), hence $p_2 = c\Psi_2'(0)\eta$. The wall derivative $\Psi_2'(0)$ is found to be $-b_0/c$ from equation (21), so that $p_2 = -b_0\eta$ or

$$p_2 = -\eta\int_0^1 \Psi_0^2(y)\,\mathrm{d}y. \tag{24}$$

Numerical examples of the real and imaginary parts of p_2/η will be given later in Figure 2 when we consider the specific velocity profile of plane Poiseuille flow.

2.4. Plane Poiseuille Flow

The general analyses of Section 2.2 indicate that (a) the shear flow exerts wave drag on the walls which could experience flutter-type instability and (b) the familiar Bernoulli effect could be reversed in laminar-like flow conditions. However, these analyses are conducted on the basis of a truncated series and for a particular value of y_c it is necessary to verify the conclusions by an exact solution for a specific velocity profile, for which purpose the plane Poiseuille flow is chosen. The parabolic velocity profile is given below, together with its critical layer level y_c,

$$U = 1-(1-y)^2, \quad y_c = 1-\sqrt{1-c}. \tag{25}$$

The integral $I(y)$ of equation (8) becomes

$$I(y) = \frac{1-y}{-2(1-c)(U-c)} + \frac{1}{4(1-c)^{3/2}} \ln\left(\frac{y-y_c}{2-y-y_c}\right).$$

The long-wave stream function $\Psi_0(y)$ of equation (8) is expressed as

$$\Psi_0(y) = \frac{2(1-y_c)(1-y) - (U-c)\ln[(y-y_c)/(2-y-y_c)]}{2(1-c)^{1/2}/c + \ln[y_c/(2-y_c)] - i\pi}. \tag{26}$$

The long-wave pressure is

$$p_0 = \frac{4(1-c)^{3/2}}{2(1-c)^{1/2}/c + \ln[y_c/(2-y_c)] - i\pi}\,\eta, \tag{27}$$

while the contribution from the k^2-term can be calculated by equation (24).

We now define the real and imaginary parts of wall pressure as the virtual stiffness K and the drag coefficient D, respectively,

$$K = \mathscr{R}e(p/\eta) = K_0 + k^2 K_2 + \cdots, \quad D = \mathscr{I}m(p/\eta) = D_0 + k^2 D_2. \tag{28}$$

K_0 and K_2 for the parabolic velocity profile are now compared with the virtual stiffness for the potential flow of the same average velocity, denoted by K_p,

$$U_{av} = \int_0^1 U(y)\,dy = \frac{2}{3}, \quad K_p = -(U_{av} - c)^2,$$

cf. equation (18). Figure 2(a) shows that $K_0 > 0$ for the whole range of wave speed, $c \in (0, 1)$, confirming our earlier anticipation that the Bernoulli effect can be reversed in laminar shear flows. The magnitude of K_0 reaches its peak at $c \approx 0.25$ instead of $c \to 0$ for K_p. Figure 2(b) shows the drag coefficients. $D_0 > 0$ means a positive wave drag or a negative fluid damping on the walls, but there is no wave drag if the mean flow is uniform. Also shown in Figure 2 are K_2 and D_2 which will be useful in the eigenvalue studies later on.

We now visualize the flow pattern for the perturbed plane Poiseuille flow for the long-wave limit. To do so we change to a reference frame that moves with the wall waves, so

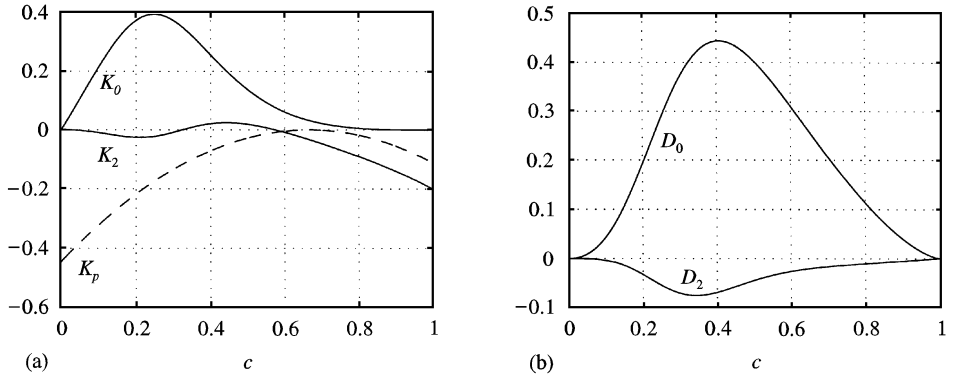

Figure 2. Virtual stiffness and damping coefficient induced by shear flow of parabolic velocity profile. (a) Comparison of the virtual stiffness K_0, K_2 with that of potential flow of the same average velocity, K_p. (b) The drag coefficients, D_0, D_2. Positive drag means negative virtual damping for the coupled fluid structural oscillation system

that the waves become stationary and the whole flow field steady. The undisturbed velocity distribution is $U - c$, so the flow goes to the left below the critical layer. Real parts of complex variables correspond to physical properties, e.g., $\eta = \eta_0 \cos(kx)$ and two wavelengths are covered for the streamline contours. The flow in Figure 3 goes to the right above the critical layer, $y > y_c = 0.15$, and to the left underneath. The closed streamline patterns are the famous Kelvin's (1880) "cat's eyes" in which flow circulates clockwise. The centres of the cat's eyes are located at a distance of 0.39 wavelength, right to the wall wave crests. This has two implications.

The first is that, since the pressure troughs are located where the wall is displaced downwards, the low pressure there tends to move the wall back to its undisturbed position, the phenomenon which we call the reversal of the Bernoulli effect. This part of the result is unique for our channel flow configuration and needs to be properly understood in simple physical terms. Figure 3(b) gives a close-up view of the streamlines near one of the Kelvin's cats' eyes. If the mean flow is uniform, then the flow is faster at the wave peaks than at the troughs. But for the shear flow, the Kelvin's cats' eyes shelter themselves in the trough region where the cross-section is enlarged, thus blocking off part of the flow passage. From Figure 3(b) it can be seen that the streamtubes are actually narrower at the trough region B than that at the peak region A. As expected, the static pressure is found to be higher where the flow is slower and the flow is slower where the streamtubes become wider. We have therefore demonstrated that the reversal of the Bernoulli effect is caused by the global change of flow pattern instead of the local breakdown of the relationship between flow velocity and static pressure.

The second implication is that the pressure has its troughs on the leeward side, so there is a component in-phase with the wave slopes causing wave drag, a result which is compatible with that obtained for shear flows in the semi-infinite space by Miles (1957) and explained by Lighthill (1962). To overcome the wave drag, the mean flow must give up part of its kinetic energy which is then fed into the growing varicose waves, a characteristic phenomenon known as flutter. The actual occurrence of flutter is now examined by the eigenvalue problem.

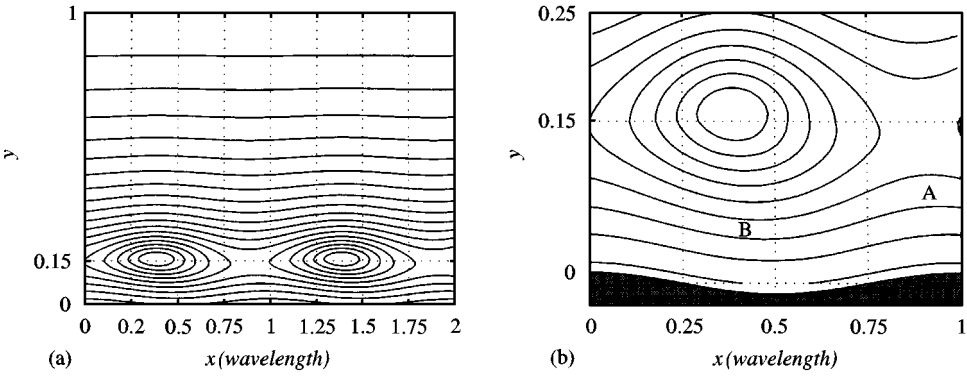

Figure 3. Streamline patterns for $y_c = 0.15$, $\eta_0 = 1\%$, $c = 0.28$. The troughs of the pressure coincide with the centres of the closed streamlines. Note that the intervals between the adjacent iso-ψ lines are less near the critical layer than elsewhere, so that more details can be shown there. (a) The overall view for two wavelengths; (b) a zoom-in around one of the Kelvin's "cats' eyes" which shows the narrowing of streamtube width from A to B. The shaded base is the wavy wall

3. THE EIGENVALUE PROBLEM

A formal solution to the dynamics of the fluid–wall eigensystem requires the knowledge of fluid loading for arbitrary wavelength. We restrict ourselves to situations where the wavelength is finite but long, so that we are reasonably confident that the inclusion of the k^2-term will give us a satisfactory approximation. We then seek to identify the parameter range in which this approximation is valid, i.e. the condition for the critical wave number to be small.

We consider a channel (see Figure 1) with its walls supported by a continuous elastic foundation. Tension and material bending stiffness can certainly be included, but our emphasis has been placed with long-wave perturbations for which the bending and tensile stresses are ineffective. The single stiffness modelling is also rather appropriate when modelling flow through collapsible tubes. Before self-induced oscillation occurs, the partially collapsed tube reacts to perturbations by developing circumferential bending stress which is often represented by a tube law, equivalent to our elastic foundation in two dimensions [method of corrections for significant longitudinal stresses can be found in McClurken *et al.* (1981)].

3.1. The Governing Equations and Approximations

The dynamics of the wall vibration is written as

$$m^*\ddot{\eta}^* + 2m^*d^*\dot{\eta}^* + E^*\eta^* + p^* = 0, \tag{29}$$

where the overdot stands for derivative with respect to time and m^*, d^*, E^*, p^* are, respectively, the dimensional mass per unit distance, damping, foundation elastance, and the wall pressure perturbations. For convenience, we also define the *in vacuo* ($p^* = 0$) oscillation frequency for a damping-free system, $\omega_0^* = \sqrt{E^*/m^*}$, which is also the critical value of the damping when the *in vacuo* oscillation frequency vanishes. The ratio of the actual damping to the critical damping,

$$d = d^*/\omega_0^*, \tag{30}$$

is the familiar damping ratio in vibration studies, although the precise mechanism of energy dissipation in solids is a complicated issue. Normally, both d^* and d are functions of frequency. But in order to focus on the fluid dynamical aspect of hydroelasticity, we simply assume that the dimensionless damping ratio d is a given material constant, bearing in mind that such assumption has certain impact on the form of the final results. To get the sense of order of magnitude for d, we consider *in vacuo* vibrations in which the amplitude decays as $\exp(-d^*t^*)$. The rate of amplitude decrease per cycle is $1 - \exp(-2\pi d) \approx 2\pi d$. Typical values of d for steel spring and natural rubber are, respectively, 0.005 and 0.05. That for living tissues is likely to be either comparable or greater than that of rubber [cf. Fung (1993)].

For a varicose wave

$$\eta^* = \eta_0^* \exp[\mathrm{i}(k^*x^* - \omega^*t^*)],$$

where $\omega^* = c^*k^*$ and k^* is real and small, the fluid loading can be written as

$$p^* = \rho_0^*(U_{\max}^*)^2(K + \mathrm{i}D)\eta^*/h^*,$$

where

$$K = K_0 + k^2 K_2 + \cdots, \quad D = D_0 + k^2 D_2 + \cdots .$$

Note that K_0, D_0, K_2 and D_2 are functions of c only, but K and D are functions of both wave speed and wave number. The equation for the dimensional complex eigenfrequency ω^* is

$$-(\omega^*)^2 - 2\mathrm{i}d^*\omega^* + (\omega_0^*)^2 + \frac{\rho_0^*(U_{\max}^*)^2}{m^* h^*}(K + \mathrm{i}D) = 0. \tag{31}$$

We now normalize the eigen-equation using the old length scale h^* but the new velocity scale $\omega_0^* h^*$. We introduce

$$m = \frac{m^*}{\rho_0^* h^*}, \quad U_w = \frac{U_{\max}^*}{\omega_0^* h^*}, \quad \omega = \frac{\omega^*}{\omega_0^*} = ckU_w, \tag{32}$$

where m is the familiar mass ratio, U_w is the centreline flow velocity scaled by the structural rigidity, and ω is the dimensionless angular velocity. Note that a factor of U_w has entered the expression for ω due to the earlier scaling of wave speed by $U_{\max}^*$. The dimensionless version of equation (29) becomes

$$-\omega^2 - 2\mathrm{i}\omega d + 1 + \frac{U_w^2}{m}(K + \mathrm{i}D) = 0.$$

Flutter occurs if the complex ω has a positive imaginary part, and the critical condition is $\mathscr{I}m(\omega) = 0$. Under the critical condition, ω is real and the eigen-equation is split into real and imaginary parts,

$$\omega^2 = 1 + \frac{U_w^2}{m}K, \quad 2\omega d = \frac{U_w^2}{m}D,$$

which clearly shows that flutter will occur when the negative fluid damping overcomes the structural damping, while a reversed Bernoulli effect will increase the eigen-vibration frequency. Inserting $\omega = ckU_w$,

$$U_w^2[(ck)^2 - K/m] = 1, \quad 2md(ck) = U_w D. \tag{33}$$

Given the mass ratio m and the damping ratio d, these two equations give two functional relationships, $U_w(k)$ and $c(k)$ between the three otherwise independent variables, c, k and U_w. The valley of the eigen-velocity curve $U_w(k)$ then gives the critical point of flutter onset. To calculate, one first needs to cancel U_w from the two equations to find the dispersion relation $c(k)$, which is then substituted back into any one of the two equations to find $U_w(k)$. This is easily done numerically. However, we found this unnecessary for flutter caused by waves of long but finite wavelength. Below we follow an approximation procedure which leads to a clear analytical solution which has been checked by accurate numerical results.

First, the cancellation of ck in the two equations (33) gives

$$U_w = \sqrt{\frac{2md}{D}}\sqrt{\varepsilon + \sqrt{\varepsilon^2 + 1}}, \quad \varepsilon = \frac{Kd}{D}. \tag{34}$$

To the long-wave limit, $\varepsilon = K_0 d/D_0$, and it can be seen from Figure 2 that K_0/D_0 is of the order of unity unless $c \to 0$, which is not the case since $ck \to 0$ will not satisfy the first of equations (33). This is so because $K_0 > 0$ and K_0/m approaches zero slower than the other

term, $(ck)^2$, as $c \to 0$. In other words, static divergence does not occur for flexible channels in which the Bernoulli effect has been reversed. The correction of finite wavelength does not have much effect on this since both K_2 and D_2 approach 0 faster then c, cf. Figure 2. Having assured that the eigenwave speed c is not too close to 0, hence $K/D = \mathcal{O}(1)$, we find the parameter $\varepsilon = \mathcal{O}(d)$, where d is small, except for materials or structures specially made for vibration absorption purposes. Therefore, equation (34) may be simplified by ignoring ε and the two equations (33) are approximated by

$$U_w \approx \sqrt{\frac{2md}{D}}, \quad \omega = ckU_w \approx 1. \tag{35}$$

It is now clear that the critical flow velocity is mainly controlled by the drag coefficient, while the influence of the virtual stiffness is practically negligible; $\omega = 1$ means $\omega^* = \omega_0^*$, i.e. resonance. One important consequence of this is that if we effectively measure the *in vacuo* frequency of the channel vibration through measuring E^* and m^*, an agreement on flutter frequency between the theoretical prediction and the experimental data does not necessarily validate the fluid dynamic model employed. The real validation can only be achieved through the flow velocity at which flutter occurs, which is not an easy task given the difficulty of modelling the structural damping mechanism accurately.

By adopting the approximation of $\varepsilon \to 0$ and recalling $D \approx D_0 + k^2 D_2$, we can solve the two equations (35):

$$k^2 = \frac{D_0}{2mdc^2 - D_2}, \quad U_w = \sqrt{\frac{2md}{D_0} - \frac{D_2}{c^2 D_0}}, \tag{36}$$

where the right-hand sides are purely functions of c. The first expression effectively gives the dispersion relationship $c(k)$ and the second will enable us to find the critical flow speed, as shown in Figure 4(a). In this example, the wave number is reasonably small and the Heisenberg expansion should converge rapidly. But Figure 4(b) shows that the method may eventually fail as md becomes too small. Therefore, $md \gg 1$ is the condition under which the long-wave features of the solution dominate the flutter behaviour. For materials like rubber,

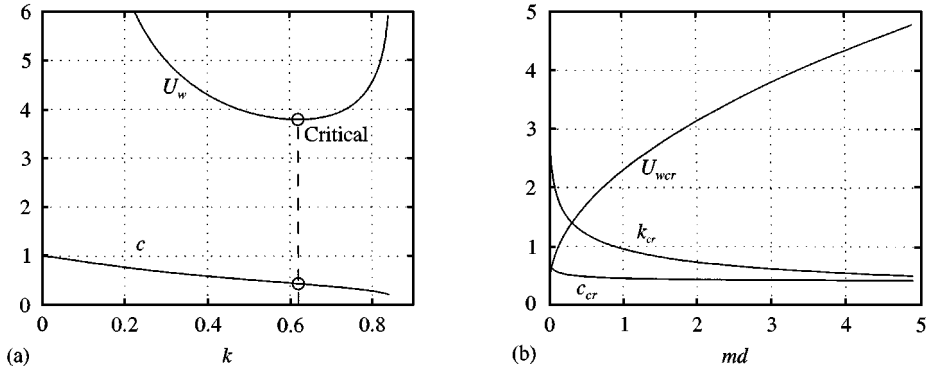

Figure 4. Eigenvalues. (a) The finding of the critical point: $m = 100$, $d = 0.06$, and the critical point is shown by a circle where $c_{cr} = 0.43$, $k_{cr} = 0.62$, $U_{wcr} = 3.79$. (b) Variation of the critical condition as a function of the controlling parameter md.

the damping ratio d is not too large, so the mass ratio, $m = m^*/\rho_0^* h^*$, has to be large. The theory is therefore valid for thick-walled and narrow channels.

Under the condition of $md \gg 1$, D_2-terms in equation (36) may be ignored, so that $U_w \approx \sqrt{2md/D_0}$. A rough estimate for flutter of very long waves should be where the long-wave drag coefficient $D_0(c)$ peaks, i.e. $c \approx 0.41$, $D_0 \approx 0.45$, cf. Figure 2(b). The approximate critical flow speed and the wave number are, respectively,

$$U_{wcr} \approx 2.12\sqrt{md}, \quad k_{cr} \approx \frac{1.16}{\sqrt{md}}.$$

Based on this simple estimate, we now revert the dimensionless results back to dimensional variables so that the influence of each physical variable can be identified clearly,

$$U^*_{max} \propto \sqrt{E^* h^* d/\rho_0^*}. \tag{37}$$

The critical flow speed increases with the elastic strength of the channel and the level of damping. The critical flow speed also increases with the channel height. Large channel wall separation stabilizes the system or the proximity of the opposing wall has a destabilizing effect.

3.2. Comparison with Larose & Grotberg's Theory

LaRose & Grotberg (1997) considered the symmetric mode instability of developing flow through flexible channels. Plane Poiseuille flow is also considered as the limit case of developing flow. They solved the eigenvalue problem of the Orr–Sommerfeld system and the numerical examples given are based on the experimental studies of Gavriely *et al.* (1989) in which the opposing walls of the partially collapsed tube are very close ($h^* = 0.7$ mm). The Reynolds number, based on the average channel flow velocity and the channel height, is 622. An analytical solution is also given for the long-wave limit. Both long-wave instability ($k = 0$) and finite wavelength flutter are found. Despite the fact that our inviscid flow model effectively takes the Reynolds number to infinity, we found agreement with their results on the following:

(i) flutter instability of symmetric mode dominates the behaviour of the flexible channels instead of the Tollmien–Schlichting instabilities;

(ii) the eigenfrequency for the thick-walled channel is close to its *in vacuo* value although, strictly speaking, our result for ω_{cr} should always be slightly over unity due to the reversal of the Bernoulli effect;

(iii) their result for the critical flow speed is in qualitative agreement with our approximate formulae (37).

However, there are differences, as follows.

(a) For our inviscid flow model, reversal of the Bernoulli effect is found for the whole range of wave speed, $c \in (0, 1)$, and therefore no long-wave instability is present in our model. However, LaRose & Grotberg were able to demonstrate that under certain conditions the long-wave instability precedes flutter when the channel height is large, which may be interpreted as the initial phase of channel collapse observed in experiments.

(b) The eigenwave speeds found in their calculations are typically twice the maximum flow speed through the channel, while ours is always less than the maximum flow speed. In other words, the critical layer where $U = c$ is absent in their studies. Their mechanism of flutter has more to do with the direct action of viscosity in the wall layer, the essence of which was modelled in the much earlier work of Grotberg & Reiss (1984). In our model, however, the main mechanism lies with the action of the critical layer and the shift of Kelvin's "cats' eyes" in relation to the varicose waves of the wall.

Being based on the inviscid flow assumption, our theory will only be a good approximation to reality when the Reynolds number (Re) at which flutter occurs is large. From equation (37) we find that the critical Reynolds number is proportional to $(h^*)^{3/2}(E^*d)^{1/2}$, depending primarily on the channel height. However, for flow through collapsible tubes, the circumferential bending stiffness, which corresponds to the foundation elastance E^* in our channel model, is related to h^* or the shortest distance between the opposing sides of the oval or dumbbell-like tube cross-section. It is beyond the scope of the present study to relate all these parameters with the gradual collapsing process of compliant tubes as the transmural pressure is raised. But we do know that the Reynolds number in the upper airways falls in the region of a few thousands, for which our inviscid flow assumption $\mathrm{Re}^{-1} \to 0$ may not be too bad after all. Of course, a more satisfactory theory has to account for the viscous effect in such an intermediate range.

3.3. Observation of Critical Wave Speed in Experiment

Experimental validation for the theoretical predictions, especially the critical flow and wave speeds, is crucial but the majority of the published experiments are not suitable for comparison for two reasons. One is that most experiments have been conducted using water as fluid [cf. Bertram *et al.* (1990)]. The mass ratio m is then relevant to applications such as blood flow through large vessels. To our knowledge, there is only one relevant experiment by Gavriely *et al.* (1989) using airflow, which was used for comparison with the theoretical predictions of LaRose & Grotberg (1997). The second reason why experimental validation of a channel flutter theory has been difficult is that the conditions under which the self-induced oscillations occur are very far from a uniform channel of great length.

The second point was highlighted by LaRose & Grotberg (1997), who showed that the flow speed through the narrow, channel-like passage of the tube is likely to be lower than that through the two side-lobes of the dumbbell-like tube section, which is also demonstrated experimentally for steady flow by Bertram & Godbole (1997). The only available velocity measurement was the total volume flow rate, or the average flow velocity through the tube. A finite element calculation was carried out by LaRose (1994) and the lower velocity through the centre sections is estimated. Direct comparison between this projected experimental data and the theoretical prediction also proved to be difficult and we do not attempt such a comparison with our prediction. What we believe would be a useful comparison, however, is the measured wave speed with the measured critical flow speed.

A range of almost 2:1 in wavelength, $\lambda^* = 3$–5 cm, was reported by Gavriely *et al.* (1989) and there are three sets of data presented by LaRose & Grotberg (1997) corresponding to the half-channel width $h^* = 0.81, 0.70, 0.37$ mm, respectively. Presumably, we may take $h^* = 0.70$ mm and $\lambda^* = 4$ cm for the purpose of estimation. For this channel width, the oscillation frequency was $f^* = 300$ Hz, so the wave speed is $c^* = \lambda^* f^* = 12$ m/s. The measured flow velocity averaged over the whole tube section was 27.60 m/s, while that for the central part was estimated by the finite element calculation as 10.0 m/s. The maximum flow speed in the channel section, however, appears to be around 20.0 m/s [cf. LaRose (1994)].

The wavelength predicted by LaRose & Grotberg (1997) was around 3 cm, corresponding to 9 m/s of wave speed for the frequency of 300 Hz, which is two to three times the predicted critical flow speed depending on the velocity profile used. The authors drew satisfaction from the fact that the predicted wave speed is close to the measured value. But from the present author's perspective, what is important in the unsteady fluid dynamics is how the

wave speed compares with the maximum flow speed in the channel, a comparison which LaRose & Grotberg did not make. On this account, we find the measured wave speed is somewhat less than the measured maximum flow speed even for flutter at such a low Reynolds number.

4. CONCLUSIONS

A boundary-value problem is investigated for the pressure perturbation induced in shear flows through channels whose walls undergo symmetric wave motions of phase speed less than the maximum flow speed. The main result is that for shear flows with moderate velocity gradient near the wall, the sign of the pressure component in phase with the wall displacement is opposite to that according to the Bernoulli equation for a uniform potential flow model. This means a reversal of the collapsing tendency of compliant fluid passages. The reversal of the Bernoulli effect can be seen as the channel–wall amplification of Miles's (1957) water wave generation mechanism. That mechanism is visualized by the right-shift of Kelvin's cat's eye flow pattern around the critical layer. It has been analytically demonstrated that, for the whole range of wave speed, $c^* \in (0, U^*_{\max})$, the parabolic profile of plane Poiseuille motion induces a right-shift in excess of a quarter wavelength, causing the reversal of the Bernoulli effect.

One of the implications is that a potential flow model does not always provide a correct first approximation to the viscous and vortical flow problems. The fact that this is so was also reflected upon by Carpenter & Garrad (1986) in their review of potential flow analyses for the study of flow stability over Kramer-type surfaces.

The second conclusion is that the fluid pressure always has a component in phase with the wave slope causing wave drag and energy transfer from the flow to the perturbation waves, a direct extension of Miles's water wave generation theory to the varicose wave in flexible channels. This is a mechanism for travelling wave flutter which occurs when the rate of this energy transfer exceeds the rate of dissipation in the walls. The eigenvalue problem is considered for the thick-walled channel flutter whose eigenwaves are likely to be long in comparison with the channel width. The critical flow velocity and the wave speed for the flutter onset are given for simply supported compliant channels. In terms of Brooke Benjamin's classification, this is a class B instability which exists even when the fluid is inviscid. Our theory therefore contrasts with a previous work (Grotberg & Reiss 1984) in which the viscous wall shear stress is fully responsible for flutter. Distinction is also made between our shear-flow flutter theory and the latest development of the viscous flutter theory (LaRose & Grotberg 1997) in which eigenwaves typically travel twice as fast as the maximum flow velocity in the channel. Further studies are needed to characterize the intermediate region in which both the wall layer and the critical layer may play important roles.

References

Bayly, B. J., Orszag, S, A, & Herbert, T. 1988 Instability mechanisms in shear-flow transition. *Annual Review of Fluid Mechanics* **20,** 359–391.

Bertram, C. D. & Godbole, S. A. 1997 LDA measurements of velocities in a simulated collapsed tube. *ASME Journal of Biomechanical Engineering* **119,** 357–363.

Bertram, C. D., Raymond, C. J. & Pedley, T. J. 1990 Mapping of instabilities for flow through collapsed tubes of different length. *Journal of Fluids and Structures* **4,** 125–153.

Brooke Benjamin, T. 1959 Shearing flow over a wavy boundary. *Journal of Fluid Mechanics* **6,** 161–205.

Brooke Benjamin, T. 1960 Effects of a flexible boundary on hydrodynamic stability. *Journal of Fluid Mechanics* **9,** 513–532.

Brooke Benjamin, T. 1963 The threefold classification of unstable disturbances in flexible surfaces bounding inviscid flows. *Journal of Fluid Mechanics* **16,** 436–450.

Cancelli, C. & Pedley, T. J. 1985 A separated-flow model for collapsible-tube oscillations. *Journl of Fluid Mechanics* **157,** 375–404.

Caro, C. G., Pedley, T. J., Schroter, R. C. & Seed, W. A. 1978 *The Mechanics of the Circulation.* Oxford: Oxford University Press.

Carpenter, P. W. & Garrad, A. D. 1985 The hydrodynamic stability of flow over Kramer-type compliant surfaces. Part 1. Tollmien–Schlichting instabilities. *Journal of Fluid Mechanics* **155,** 465–510.

Carpenter, P. W. & Garrad, A. D. 1986 The hydrodynamic stability of flow over Kramer-type compliant surfaces. Part 2. Flow-induced surface instabilities. *Journal of Fluid Mechanics* **170,** 199–232.

Conrad, W. A. 1969 Pressure–flow relationships in collapsible tubes. *IEEE Journal of Biomedical Engineering* **16,** 284–295.

Davies, C. & Carpenter, P. W. 1997 Numerical simulation of the evolution of Tollmien-Schilichting waves over finite compliant panels. *Journal of Fluid Mechanics* **335,** 361–392.

Fung, Y. C. 1993 *Biomechanics*: *Mechanical Properties of Living Tissues.* New York: Springer-Verlag.

Gavriely, N., Shee, T. R., Cugell, D. W. & Grotberg, J. B. 1989 Flutter in flow-limited collapsible tubes: a mechanism for generation of wheezes. *Journal of Applied Physiology* **66,** 2251–2261.

Green, C. H. & Ellen, C. H. 1972 The stability of plane Poiseuille flow between flexible walls. *Journal of Fluid Mechanics* **51,** 403–416.

Grotberg, J. B. & Reiss, E. L. 1984 Subsonic flapping flutter. *Journal of Sound and Vibration* **92,** 349–361.

Grotberg, J. B. & Shee, T. R. 1985 Compressible-flow channel flutter. *Journal of Fluid Mechanics* **159,** 175–193.

Grotberg, J. B. & Gavriely, N. 1989 Flutter in collapsible tubes: a theoretical model of wheezes. *Journal of Applied Physiology* **66,** 2262–2273.

Grotberg, J. B. 1994 Pulmonary flow and transport phenomena. *Annual Review of Fluid Mechnics* **26,** 529–571.

Hains, F. D. & Price, J. F. 1962 Effect of a flexible wall on the stability of Poiseuille flow. *Physics of Fluids* **5,** 365–365.

Heil, M. & Pedley, T. J. 1996 Large post-buckling deformations of cylindrical shells conveying viscous flow. *Journal of Fluids and Structures* **10,** 565–599.

Huang, L., Quinn, S. J., Ellis, P. D. M. & Ffowcs Williams, J. E. 1995 Biomechanics of snoring. *Endeavour* **19,** 96–100.

Jensen, O. E. 1990 Instabilities of flow in a collapsed tube. *Journal of Fluid Mechanics* **220,** 623–659.

Kamm, R. D. & Pedley, T. J. 1989 Flow in collapsible tubes: a brief review. *ASME Journal of Biomechanical Engineering* **111,** 177–179.

Kececioglu, I., McClurken, M. E., Kamm, R. D. & Shapiro, A. H. 1981 Steady, supercritical flow in collapsible tubes. Part 1. Experimental observations. *Journal of Fluid Mechanics* **109,** 367–389.

Kelvin, Lord 1880 On a disturbing infinity in Lord Rayleigh's solution for waves in a plane vortex stratum. *Nature* **XXIII,** 45–46.

Kramer, M. O. 1957 Boundary layer stabilization by distributed damping. *Journal of the Aerospace Sciences* **24,** 459.

Kumaran, V., Fredrickson, G. H. & Pincus, P. 1994 Flow-induced instability at the interface between a fluid and a gel at low Reynolds number. *Journal of Physics Paris II* **4,** 893–904.

Kumaran, V. 1995*a* Stability of the viscous flow of a fluid through a flexible tube. *Journal of Fluid Mechanics* **294,** 259–281.

Kumaran, V. 1995*b* Stability of the viscous flow of a fluid through a flexible tube at high Reynolds number. *Journal of Fluid Mechanics* **302,** 117–139.

Kumaran, V. 1996 Stability of inviscid flow in a flexible tube. *Journal of Fluid Mechanics* **320,** 1–17.

LaRose, P. G. 1994 Wall-fluid instabilities in compliant channels conveying developing flows. Ph.D. Thesis, Northwestern University, U.S.A.

LaRose, P. G. & Grotberg, J. B. 1997 Flutter and long-wave instabilities in compliant channels conveying developing flows. *Journal of Fluid Mechanics* **331,** 37–58.

Landahl, M. T. 1962 On the stability of a laminar incompressible boundary layer over a flexible surface. *Journal of Fluid Mechanics* **13,** 609–632.

Lighthill, M. J. 1962 Physical interpretation of the mathematical theory of wave generation by wind. *Journal of Fluid Mechanics* **14,** 385–398.

Lin, C. C. 1955 *The Theory of Hydrodynamic Stability*. Cambridge: Cambridge University Press.

Luo X. Y. & Pedley, T. J. 1996 A numberical simulation of unsteady flow in a two-dimensional collapsible channel. *Journal of Fluid Mechanics* **314,** 191–225.

McClurken, M. E., Kececioglu, I., Kamm, R. D. & Shapiro, A. H. 1981 Steady, supercritical flow in collapsible tubes. Part 2. Theoretical studies. *Journal of Fluid Mechanics* **109,** 391–415.

Matsuzaki, Y. & Fung, Y. C. 1979 Non-linear stability analysis of a two-dimensional model of an elastic tube conveying a compressible flow. *Journal of Applied Mechanics* **46,** 31–36.

Miles, J. W. 1957 On the generation of surface waves by shear flows. *Journal of Fluid Mechanics* **3,** 185–204.

Miles, J. W. 1959 On the generation of surface waves by shear flows, Part 2. *Journal of Fluid Mechanics* **6,** 568–582.

Miles, J. W. 1962 On the generation of surface waves by shear flows, Part 4. *Journal of Fluid Mechanics* **13,** 433–448.

Nguyen, V. B., Païdoussis, M. P. & Misra, A. K. 1993 An experimental study of the stability of cantilevered coaxial cylindrical shells conveying fluid. *Journal of Fluids and Structures* **7,** 913–930.

Nguyen, V. B., Païdoussis, M. P. & Misra, A. K. 1994 A CFD-based model for the study of the stability of cantilevered coaxial cylindrical-shells conveying viscous-fluid. *Journal of Sound and Vibration* **176,** 105–125.

Païdoussis, M. P. & Issid, N. T. 1974 Dynamic stability of pipes conveying fluid. *Journal of Sound and Vibration* **33,** 267–294.

Rotenberry, J. M. 1992 Finite-amplitude shear waves in a channel with compliant boundaries. *Physics of Fluids* A **4,** 270–276.

Rotenberry, J. M. & Saffman, P. G. 1990 Effect of compliant boundaries on weakly nonlinear shear waves in channel flow. *SIAM Journal of Applied Mathematics* **50,** 361–394.

Shapiro, A. H. 1977 Steady flow in collapsible tubes. *ASME Journal of Biomechanical Engineering* **99,** 126–147.

Weaver, D. S. & Païdoussis, M. P. 1977 On collapse and flutter phenomena in thin tubes conveying fluid. *Journal of Sound and Vibration* **50,** 117–132.